Extreme lowering of the Debye temperature of Sn nanoclusters embedded in thermally grown SiO_2 by low-lying vibrational surface modes

G. E. J. Koops,* H. Pattyn, A. Vantomme, S. Nauwelaerts, and R. Venegas†
Instituut voor Kern- en Stralingsfysica, Physics Department, K. U. Leuven, Celestijnenlaan 200D, B-3001 Leuven, Belgium
(Received 15 December 2003; revised manuscript received 17 September 2004; published 8 December 2004)

The formation and dynamical behavior of Sn clusters embedded in amorphous, thermally grown SiO_2 layers, formed by ion implantation, is monitored through ^{119}Sn Mössbauer spectroscopy. We observe an extreme decrease of the cluster Debye temperature θ_D for samples annealed at 800 °C in a reducing atmosphere. We show with a model, based on classical elasticity theory, that this lowering can be explained by a decrease of the surface vibrational modes when a Sn microcrystal is embedded in a SiO_2 matrix.

DOI: 10.1103/PhysRevB.70.235410 PACS number(s): 61.18.Fs, 61.46.+w, 62.30.+d, 63.22.+m

I. INTRODUCTION

In recent years, ion implantation has been used to introduce foreign ions into pure or thermally grown silica to form nanoclusters.[1] An attractive feature of ion implantation to form these nanoclusters is that the clusters grow in a well-defined region in the sample, determined by the implantation depth. Most of the scientific effort is focussed on the interesting linear and nonlinear optical properties of these layers which can have applications in optical semiconducting devices such as lasers based on Si technology.[2] The combination of ion implantation and thermally grown SiO_2 is in this respect quite promising since both techniques are employed on a massive scale in semiconductor industry. The physical properties of these nanocrystals differ largely from the normal bulk ones. This can be attributed to both the discreteness of the electronic states for very small clusters as well as to the large influence of the surface of the particle due to its large surface to volume ratio.

Also the vibrational dynamics of the particle change drastically in going to very small cluster sizes. This change will reflect in some of the physical properties of the precipitates such as the thermal heat capacity, the superconducting transition temperature, the melting temperature, and the Mössbauer *f* fraction. Processes governed by electron-phonon interactions (such as superconductivity) are also influenced by the change in the vibrational spectrum.

Numerous attempts have been made to give a good theoretical description for the vibrations of free and embedded nanoclusters, mostly in connection with the effect of the particle size on the specific heat and the Debye-Waller factor. These descriptions are based on a wide variety of models such as the Einstein model,[3] the dynamical matrix model,[4] molecular dynamics,[5] and the elastic-body model.[6] The last model has been especially successful in describing the low-lying vibrational modes for embedded nanoclusters as was shown by low-frequency Raman scattering data.[7–12] This model is very powerful in describing the complete physical behavior of a microcrystal embedded in a matrix since it can calculate all vibrational modes with only a few material parameters (the longitudinal and transversal velocity of sound and the density for the cluster and matrix material).

In the present paper we present experimental evidence for a dramatic decrease in the Debye temperature (θ_D) for Sn particles embedded in a SiO_2 matrix with sizes between 3 and 4 nm. This effect is in good agreement with elasticity calculations based on the theory of Tamura *et al.*[6]

II. EXPERIMENT

The Mössbauer spectroscopy technique was chosen to study the dynamics of the metallic Sn clusters. This technique is superb for the study of these kind of problems since an extremely small amount of material needs to be measured (1.5×10^{16} at/cm^2). Another major advantage is the fact that the substrate has no influence on the measurement and the measured signal fully originates from the clusters.

A layer of 850 Å of SiO_2 was thermally grown on a 10 mm $\times$ 10 mm Si⟨100⟩ substrate, using a dry oxidation process. Subsequently, the layers were implanted with a combination of the stable ^{119}Sn isotope and the radioactive ^{119m}Sn isotope to produce samples which can be used as sources in our Mössbauer experiments. The implantation energy was chosen to be 80 keV. With that energy the maximum projected range of the Sn^+ ions falls within the SiO_2 layer and no ions are implanted into the Si substrate. All implantations were done at RT.

The samples were subjected to an isochronal annealing treatment of 20 min in a reducing gas flow, consisting of 5N H_2+N_2. The gas was led through a trap cooled with liquid N_2 in order to eliminate any moisture contamination. The annealing steps were 500, 600, 700, 750, 800, and 900 °C, respectively.

The sample is mounted as a source on a Mössbauer drive and put in an exchange-gas cryostat. Measuring temperatures are 4, 77, and RT. The radiation is detected outside the cryostat with a resonant scintillation detector of the type RITVERC RSD.221. This type of detector only measures the resonant, recoilless radiation from the source and is almost insensitive to all other radiation. In this way, a very efficient way of counting the radiation is achieved. The resonating material in the scintillator is $CaSnO_3$ and all isomer shifts are given relative to this standard. One has to keep in mind that with this special setup of the resonant detector, the minimum experimental linewidth is the convential Mössbauer linewith of $2\Gamma_0$—hence it is not lowered to $1.47\Gamma_0$ as is the usual case when measuring with a resonant detector.[13] This is caused by

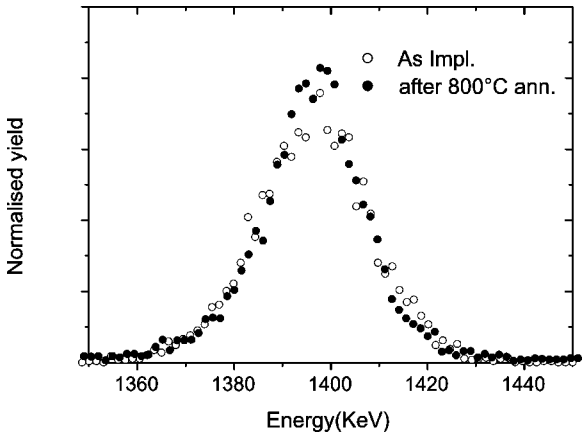

FIG. 1. RBS measurements on the sample with a Sn dose of 1.5×10^{16} at/cm^2. The open dots are for the as-implanted situation while the solid dots are measured after annealing at 800 °C. For clarity only the Sn peak is shown.

the fact that the detector is not used in resonance but rather as a very selective counter for the radiation coming from the ^{119}Sn Mössbauer transition.

III. RESULTS AND DISCUSSION

A. RBS results

A complete set of Mössbauer and RBS measurements were performed on a sample with a total implanted dose of 1.5×10^{16} Sn/cm^2. Two RBS measurements on this sample are shown in Fig. 1. We see almost no redistribution of the Sn through the SiO_2 layer in this sample upon annealing. Only a small fraction of the Sn moves from the SiO_2 surface to the central part of the implantation profile. TEM measurements (not shown) confirm this behavior. In the TEM pictures we can see a distribution of clusters with diameters of 3 to 4 nm around the initial implantation profile. These results are in sharp contrast with measurements reported by other groups on Sn nanoclusters[14–16] and Ge nanoclusters in SiO_2.[17–20] They performed the annealing in a nonreducing enviroment using Ar or dry N_2 as an annealing ambient. Their measurements show a trimodal Sn redistribution through the SiO_2 layer. Borodin[20] explains this effect using a model which takes into account the indiffusion of O_2 and H_2O from the annealing ambient into the SiO_2 layer. The effective removal of these impurities and the use of a reducing gas in our thermal treatment of the samples strongly suppress this redistribution effect, leading to this Gaussian Sn profile as shown in Fig. 1.

B. Mössbauer results

In our measurements, the sample under investigation is used as a moving source while the resonant detector is functioning as absorber as well as detector at the same time. In this way essentially only recoilless radiation is measured by the detector. At a given temperature, the mean-squared vibrational amplitude (MSVA) $\langle x^2\rangle$ of the radiating Mössbauer

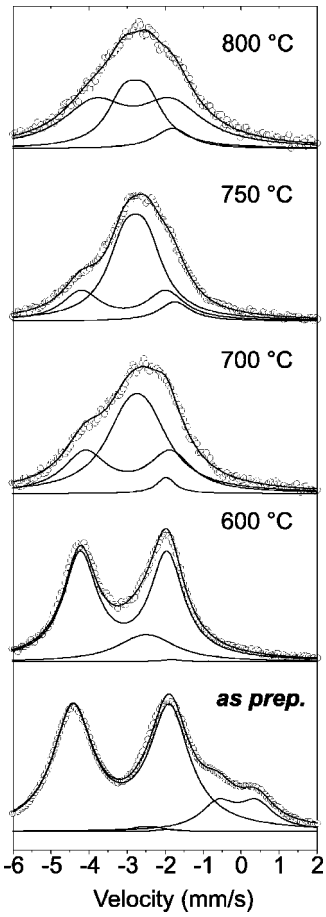

FIG. 2. Mössbauer spectra measured at 77 K for some annealing steps. We show the fitted curve together with the decomposition in spectral components. Since the sample is the source for these Mössbauer measurements, the isomer shifts are situated at negative values. To compare these values with the literature one has to change the sign of the given isomer shifts.

atoms dertermines the fraction f of atoms that participate in the recoilless emission and therefore determines the line intensity of each Mössbauer component

$$f=\exp(-k^2\langle x^2\rangle)=\exp\left(-k^2\left\langle\frac{u^2}{3}\right\rangle\right), \tag{1}$$

where $\langle x^2\rangle$ is the component of the msva in the direction **k** of the γ emission with wave number k and $\langle u^2\rangle$ is the total MSVA. Assuming a Debye phonon distribution, the temperature dependence of the f fraction is given by

$$f=\exp\left\{-\frac{9k^2\hbar^2}{Mk_B\theta_D}\left[\frac{1}{4}+\left(\frac{T}{\theta_D}\right)^2\int_0^{\theta_D/T}\frac{xe^x}{e^x-1}dx\right]\right\}. \tag{2}$$

Using Eq. (2) we can fit the temperature-dependent Mössbauer line intensities with θ_D as a fitting parameter.

1. Components and site population

The Mössbauer spectra measured at 77 K for some selected steps are shown in Fig. 2. In general we can fit the spectra with four different, well resolved components. Table

TABLE I. Fitted Mössbauer parameters for the spectra shown in Fig. 2. All isomer shifts are given with respect to $CaSnO_3$.

Temp.	Comp.	δ(mm/s)	Δ(mm/s)	Γ(mm/s)
as. impl.	Sn^{4+}	−0.10(4)	1.00(5)	1.12(12)
	Sn^{2+}	−3.15(4)	2.53(2)	1.28(4)
	β-Sn	−2.47(8)	0.42(12)	0.64(24)
	Sn/Si	−1.90(10)	0	1.14(12)
600 °C	Sn^{2+}	−3.09(2)	2.28(2)	1.08(4)
	β-Sn	−2.49(6)	0.42(10)	1.66(9)
	Sn/Si	−1.84(12)	0	1.18(20)
700 °C	Sn^{2+}	−2.98(5)	2.24(3)	1.38(3)
	β-Sn	−2.73(7)	0.53(6)	1.48(14)
	Sn/Si	−1.97(8)	0	1.16(13)
750 °C	Sn^{2+}	−3.01(8)	2.24(7)	1.20(8)
	β-Sn	−2.70(5)	0.42(5)	1.38(16)
	Sn/Si	−2.19(10)	0	1.14(7)
800 °C	Sn^{2+}	−2.74(7)	2.30(5)	1.96(15)
	β-Sn	−2.71(5)	0.60(4)	1.02(12)
	Sn/Si	−1.94(8)	0	1.00(13)

I gives a summary of the fitted Mössbauer parameters.

The first component, only present in the as implanted and 500 °C annealed sample (not shown), is centered around 0 mm/s and is Sn in a Sn^{4+} configuration, most probably Sn bounded to two oxygen atoms as in SnO_2. The isomer shift (δ) as well as the quadrupole splitting (Δ) value of this site are close to the ones of c-SnO_2, −0.02, and 0.5 mm/s, respectively,[21] and to the values measured in a-SnO_2, 0.129 and 0.70 mm/s, respectively.[22] The second component has a large δ and a large Δ and scatters around the a-SnO isomer shift value of 2.87 mm/s (Ref. 22) with a tendency to even larger values, such as were observed in Sn^{2+} molecules formed in amorphous float glass.[23] The quite large linewidth of this component is a strong indication that this site is a distribution of closely related Sn^{2+} (SnO_x) configurations.

The third component is a very small single line and makes up only 3% of the absolute site population. Its δ scatters around 1.9 mm/s which is an indication of Sn in a covalent, cubic surrounding. From the Mössbauer parameters alone this component could be either α-Sn or Sn in a fourfold coordinated Si environment. If we consider the derived Debye temperatures (see below) we may attribute this component to the latter possibility. The last component has a widely varying δ between 2.47 and 2.73 mm/s and a Δ of 0.5 mm/s. These values are close to, but significantly different from the reference values measured for bulk β-Sn of $\delta = 2.56$ mm/s and $\Delta = 0.3$ mm/s.[21,24] Especially the larger Δ values point to the precipitation of Sn in small β-Sn clusters. A more detailed description for the shifted values of the β-Sn isomer shift can be found in Ref. 25.

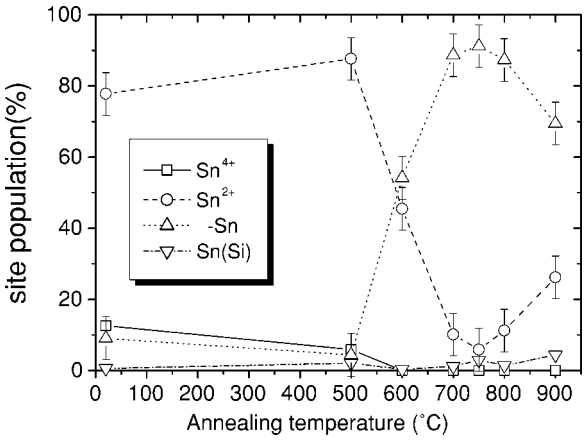

FIG. 3. Absolute site population for the sample with an initial Sn concentration of 1.5×10^{-16} at./cm^2. The f fraction for each component is determined from temperature-dependent measurements.

From temperature-dependent measurements we can determine the f fraction for each of these components using Eq. (2). The absolute site population of each component is then determined and is plotted in Fig. 3.

The first clear changes take place after annealing at 600 °C. The Sn^{2+} component disappears to make place for the β-Sn component. At this annealing temperature both components each populate around 50% of the sites. At higher temperatures more than 90% of the atoms end up in a β-Sn surrounding. Annealing temperatures of 900 °C and above causes the β-Sn component to oxidize slowly, which is accompanied by an increase of the SnO_x component.

2. Temperature-dependent measurements

The β-Sn component shows a unique behavior in the temperature-dependent Mössbauer measurements. The Mössbauer spectra at 4, 77, and 295 K after a 800 °C annealing step are shown in Fig. 4. For all three spectra the isomer shift, quadrupole splitting and linewidth are fitted consistently so they are the same for all spectra. The second-order Doppler shift, calculated from the derived Debye temperature θ_D, is taken into account in the consistent iterative fitting procedure.

The Debye temperature θ_D for each component is derived from a fit with Eq. (2). The results are shown in Table II, together with some literature values for comparison. The Debye fit for the β-Sn component is shown in Fig. 5(a).

The temperature dependence of the spectrum is fully determined by the behavior of the β-Sn component. At 4 K this component makes up more than 90% of the spectral weight while the spectral weight is reduced to zero at RT. The resulting Debye temperature of 82 K is quite insensitive to the precise fitting procedure and the component assignment. This extreme reduction of the cluster Debye temperature is a huge effect and one of the largest measured on metallic nanoclusters. The vibrational amplitude of the atoms in the cluster is 70% larger than in bulk β-Sn.

A logical explanation of this lowering of the f fraction and therefore the apparent lowering of the Debye tempera-

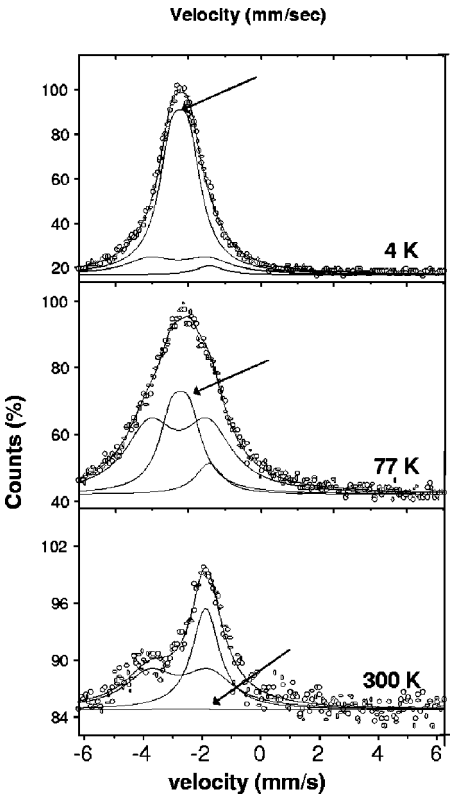

FIG. 4. Temperature-dependent Mössbauer measurements of the 1.5×10^{16} at./cm^2 sample. The sample is annealed at 800 °C and the spectra are consistently fitted where the second-order doppler-shift is taken into account. The expected position of the β-Sn component is indicated with an arrow.

ture could be a strong reduction of the melting temperature of the Sn nanoclusters since the f fraction of a liquid reduces to zero. A strong decrease of the melting temperature of nanocrystalline β-Sn has already been predicted and measured by several authors.[30–34] A lowering of the melting temperature by more than 100 K has been measured on very small isolated Sn clusters ($N\sim500$) (Ref. 31) while even bigger reductions are predicted by thermodynamical models.[34] In order to verify this assumption, we have performed constant velocity Mössbauer measurements at temperatures between 4.2 and 30 K. With this technique only two different velocities are used to measure the intensity of a Mössbauer peak, one of the velocities is exactly the β-Sn resonance velocity and the other is a random velocity far from any resonance. In this way we can measure in a very fast way the temperature dependence of the β-Sn component. We only need to correct this intensity for the overlapping intensity of the SnO_x component at the β-Sn resonance

TABLE II. Derived Debye temperatures from Fig. 4.

Comp	θ_D	Literature
β-Sn	82(8)	140 K (Ref. 26), 143 K (Ref. 27)
Sn(Si)	220(20)	230 K (Refs. 27 and 28)
Sn^{2+}	135(15)	180 K (Ref. 29) (for float-glass)

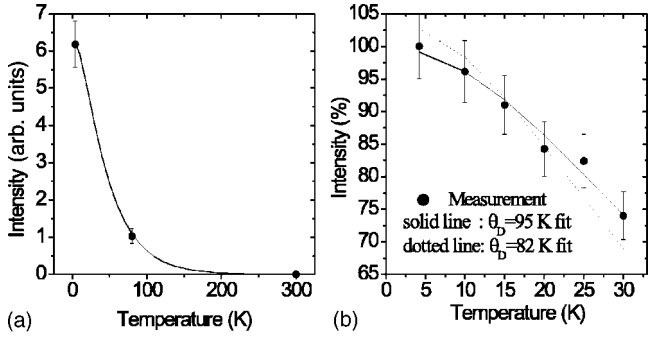

FIG. 5. (a) The measured temperature-dependent intensities for the β-Sn component of the spectra from Fig. 4, fitted with the Debye model. The fit results in $\theta_D=82(8)$ K. (b) Temperature-dependent intensities of the β-Sn component in the low-temperature constant-velocity experiments. The values are corrected for the intensity of the SnO_x component at the β-Sn resonance velocity. The fit (full line) gives $\theta_D=95(9)$ K. The dotted line is the best fit if we keep θ_D fixed at 82 K.

velocity. This correction can be made since from our temperature-dependent measurements we know the Debye temperature and the Mössbauer parameters for this component and therefore the temperature-dependent intensity at the β-Sn resonance velocity. These results are shown in Fig. 5 and give a θ_D of 95 K which confirms the strong reduction from the bulk value of 142 K. We conclude from this set of measurements that even the f fractions at low temperature are strongly reduced compared to the bulk β-Sn values. Since the Debye temperature in this case is determined at very low temperatures, well below the lowest possible reduced melting temperature predicted by the models of Lai,[34] we can rule out the reduction of the melting temperature as an explanation of our measurements.

C. The elastic continuum model

In order to model the vibrational behavior of our nanoclusters and to get some better understanding of the obtained results, we will use a model based on classical elasticity theory. In this model the cluster is assumed to be an isotropic, homogeneous, elastic body, embedded in a homogeneous elastic matrix material. Knowledge of the macroscopic parameters of both materials allows one to use classical elasticity theory to calculate the vibrational dynamics of the embedded cluster. This model has recently proven to be very successful in describing the low-lying vibrational modes of embedded nanoclusters measured by low-frequency Raman scattering.[7–12] The frequency equations for a free (nonembedded) cluster were described by Lamb[35] while the frequency equations for an embedded cluster were first given by Tamura *et al.*[6] Some small errors in the latter equations were corrected by Ovsyuk and Novikov.[9] These calculations show that two acoustic phonon modes (σ=spheroidal or torsional) can be obtained in a spherical nanocluster. Their eigenfrequencies are characterized by two quantum numbers n and l. The $n=0$ modes are the surface vibrational modes while the solutions for $n\geqslant1$ are the inner modes. The only input parameters of the model are the macroscopic longitudinal and

TABLE III. Material constants used for the calculation of the vibrational modes of free and embedded Sn clusters.

Material	ρ(g/cm^3)	v_l(m/s)	v_t(m/s)	Mass(a.u.)
Sn	7349	3532	2007	118.7
SiO_2	2426	5642	3280	60.1

tranversal velocity of sound (v_l and v_t, respectively) and the mass density (ρ) for the cluster as well as for the matrix material. If all frequency modes ω_{nl}^{σ} are calculated, we can derive the mean-squared vibrational amplitude of the clusters in the continuum aproximation using Eq. (3):

$$\langle u^2\rangle_T = \frac{3\hbar}{8\pi\rho R^2 v_t}\sum_{\sigma}\sum_{\eta_{nl}^{\sigma}}\sum_{l}\frac{(2l+1)}{\eta_{nl}^{\sigma}}\coth\left(\frac{\eta_{nl}^{\sigma}}{2\tau}\right), \qquad (3)$$

where ρ is the density of the cluster material, R is the cluster radius, v_t is the transversal velocity of sound in the cluster material, $\eta_{nl}^{\sigma}=(R/v_t)\omega_{nl}^{\sigma}$, $\tau=(k_BR/\hbar v_t)T$, k_B is Boltzmann's constant. The summation is over all the l states, all the frequencies, and the spherical and torsional modes. Note that the cluster size is only entering the equations in the calculation of the mean square vibrational amplitude. The frequency modes ω_{nl}^{σ} are size independent. We also have to put a restriction on the maximum value for l, $l_{\max}$, and the maximal vibrational mode η_{nl}^{σ}. The wavelength around a sphere is given by $2\pi/\left(l+\frac{1}{2}\right)$ while the smallest possible wavelength is $2d$ with d the smallest interatomic distance in the bulk material. The maximal angular momentum l is therefore given by

$$l_{\max} = \pi(r/d) - \frac{1}{2}. \qquad (4)$$

The maximal number of frequencies is given by the restriction that the total number of frequencies cannot be higher than the number of degrees of freedom $3N$, where N is the number of atoms in the cluster. We use the cutoff condition suggested by Tamura[36]

$$\sum_{\eta,l}(2l+1) = 2N \quad \text{for the spherical modes} \qquad (5)$$

and

$$\sum_{\eta,l}(2l+1) = N \quad \text{for the torsional modes.} \qquad (6)$$

By calculating the MSQA with Eq. (3), we can determine the f fraction f at each temperature with Eq. (1). We can subsequently solve Eq. (2) to extract the Debye temperature θ_D for each annealing temperature. Equation (3), used for calculating the MSVA $\langle u^2\rangle$, assumes some approximations which we have to keep in mind when we want to interpret the results of this model. First, in calculating the f fraction for a cluster of a certain size, we assume that $\langle u^2\rangle$ is the same for all the atoms in the cluster. This is, in general, a good approximation for the higher-lying modes (large n) but the lowest modes ($n=0$) are surface modes and the movements of these atoms are restricted to the first 2 or 3 atomic layers of the cluster. In calculating the f fraction we therefore overestimate the influence of the surface modes since we consider them present for all the atoms in the cluster. This problem can be solved by calculating $\langle u^2\rangle$ as a function of the radius r as has been done for the torsional surface modes by Ovsyuk.[9] Doing so for all the modes is a computational demanding task and we therefore used the approximation of Eq. (3). Secondly, the Bose summation assumes semiclassical (statistical) mechanics for the oscillators and their energies. For very small clusters and low temperatures we can have deviations from this semiclassical behavior. These corrections are small for our temperature range of interest and are therefore omitted.

D. Theoretical results and discussion

We have performed calculations to compute the full vibrational spectrum for free Sn nanoclusters and Sn nanoclusters

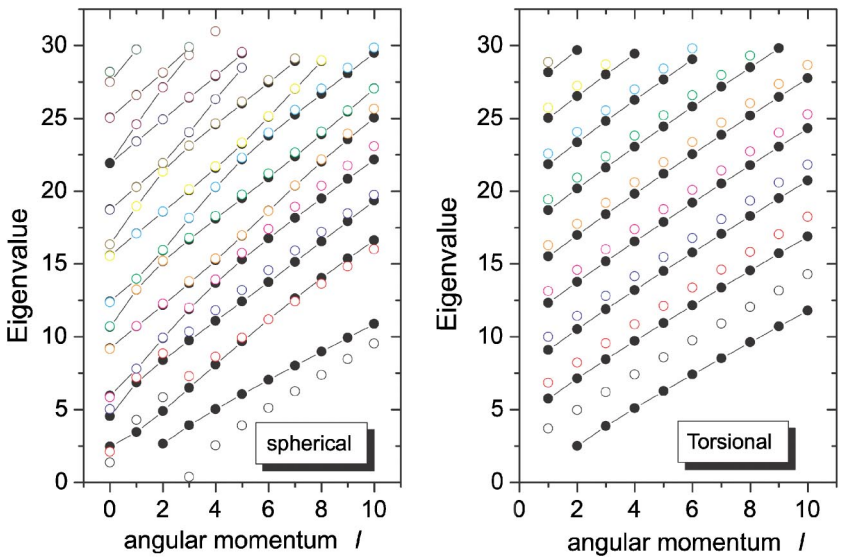

FIG. 6. Lowest-lying vibrational modes for a Sn particle in a SiO_2 matrix (open dots). For comparison, the modes for a free cluster are shown as well (black dots).

embedded in a SiO_2 matrix. The elastic constants and densities for both materials are given in Table III.

These material constants are the only necessary input parameters for the model. The calculated solutions of the frequency equation for the spherical as well as for the torsional modes are plotted in Fig. 6. The solutions for both the free and embedded clusters are given in one graph. Only the lowest modes with an angular momentum of 10 or smaller are shown. The spherical solutions clearly show that the set of lowest modes (the $n=0$ surface modes) of the embedded clusters are lowered compared to the surface modes of the free cluster.

On the contrary, for the torsional modes, the surface mode of the embedded cluster is raised compared with the modes of a free Sn cluster. The lowering of the spherical modes with the lowest l values is so effective that this will fully determine the f fraction behavior in our Mössbauer experiments. This behavior is clearly demonstrated in Fig. 7 where we have plotted the Mössbauer f fraction as a function of the temperature if we leave the 1, 2, 3, or 10 lowest states out of the calculation. The paramount influence of the lowest mode is now obvious. By raising the cluster size, the amount of available states is increasing with R^3. Therefore the low-lying state will become less important and eventually the f fraction will reach the bulk value for β-Sn.

From the fact that Sn is a "soft" material (low θ_D) and SiO_2 is a "hard" material (high θ_D), we would expect that the embedded Sn clusters would harden, i.e., show a lower $\langle x^2 \rangle$ compared to a free Sn cluster. Both our measurements and calculations show however that it is possible to create specific low-lying surface modes that soften the cluster upon embedment. This softening has been noticed in similar calculations by Ovsyuk[9] where they stated that the spherical surface vibrations with $l=0,2,3$ can soften if the stiffness of the matrix increases. These surface modes can even disappear for certain values of the elastic constants for the matrix and the cluster. This softening of the modes with increasing matrix stiffness is not a general rule but depends in complex ways on the material parameters for the cluster and the matrix material. The similar system of a Pb particle in a glass matrix, as described in the original paper of Tamura *et al.* where he applied the ECM model for embedded clusters for the first time,[6] does not exhibit a lowering of eigenfrequencies. In that specific case the surface modes of the particle disappear completely.

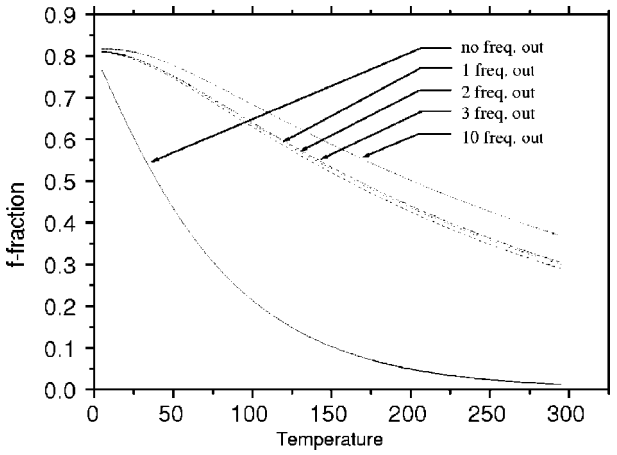

FIG. 7. The f fraction as a function of temperature if we leave the 1, 2, 3, or 10 lowest states from the solutions in Fig. 6 out of the calculation.

IV. CONCLUSIONS

Using Mössbauer spectroscopy we have been able to measure a shift in the phonon density of states of metallic Sn clusters embedded in thermally grown SiO_2. This shift creates a specific low-lying surface mode that strongly softens the cluster upon embedment and has a very large effect on the vibrational amplitude of the atoms in the cluster. The Debye temperature changes from 140 to 82 K which gives a 70% increase in the vibrational amplitude of the cluster atoms. These measurements can be explained by an elastic continuum model, based on macroscopic material parameters, which describes the vibrational spectrum of embedded spherical clusters in detail.

ACKNOWLEDGMENTS

We would kindly like to thank Andre Stesmans for the preparation of the thermal oxide layers. This work was supported by the PAI/IUAP Contracts No. 4/10, 5/1, and by a Flemish-Chilian bilateral collaboration, Project No. 96/42.

*Present address: Philips Research Leuven, Kapeldreef 75 (D1), B-3001, Leuven, Belgium; Email address: gerhard.koops-@philips.com

†Work performed while on leave from University of Santiago, Chile.

[1] H. Hosono, Jpn. J. Appl. Phys., Part 1 **32**, 3892 (1993).

[2] L. Pavesi, L. D. Negro, C. Mazzoleni, G. Franzò, and F. Priolo, Nature (London) **408**, 440 (2000).

[3] J. Childress, C. C. A. M. Zhou, and P. Sheng, Phys. Rev. B **44**, 11 689 (1991).

[4] H. Smit, P. Nugteren, R. Thiel, and L. D. Jongh, Physica B **153**, 33 (1988).

[5] M. Hou, M. E. Azzaoui, H. Pattyn, J. Verheyden, G. Koops, and G. Zhang, Phys. Rev. B **62**, 5117 (2000).

[6] A. Tamura, K. Higeta, and T. Ichinokawa, J. Phys. C **15**, 4975 (1982).

[7] A. Tanaka, S. Onari, and T. Arai, Phys. Rev. B **47**, 1237 (1993).

[8] M. Montagna and R. Dusi, Phys. Rev. B **52**, 10 080 (1995).

[9] N. Ovsyuk and V. Novikov, Phys. Rev. B **53**, 3113 (1996).

[10] A. Dièguez, A. Romano-Rodriguez, J. R. Morante, N. Bârsan, U. Weimar, and W. Göpel, Appl. Phys. Lett. **71**(14), 1957 (1997).

[11] P. Verma, W. Cordts, G. Irmer, and J. Monecke, Phys. Rev. B **60**, 5778 (1999).

[12] X. Wu, Y. Mei, G. Siu, K. Wong, K. Moulding, M. Stokes, C. Fu,

and X. Bao, Phys. Rev. Lett. **86**, 3000 (2001).
[13] K. Mitrofanov, N. Illarionova, and V. S. Shpinel, Prib. Tekh. Eksp. **3**, 49 (1963).
[14] A. Markwitz, R. Grötzschel, K. Heinig, L. Rebohle, and W. Skorupa, Nucl. Instrum. Methods Phys. Res. B **152**, 319 (1999).
[15] A. Nakajima, T. Futatsugi, N. Horiguchi, and N. Yokoyama, Appl. Phys. Lett. **71**, 3652 (1997).
[16] A. Nakajima, T. Futatsugi, H. Nakao, T. Uuki, N. Horiguchi, and N. Yokoyama, J. Appl. Phys. **84**, 1316 (1998).
[17] J. V. Borany, R. Grötzschel, K. Heinig, A. Markwitz, W. Matz, B. Schmidt, and W. Skorupa, Appl. Phys. Lett. **71**, 3215 (1997).
[18] K. Heinig, B. Schmidt, A. Markwitz, R. Grötzschel, M. Strobel, and S. Oswald, Nucl. Instrum. Methods Phys. Res. B **148**, 969 (1999).
[19] A. Markwitz, L. Rebohle, H. Hofmeister, and W. Skorupa, Nucl. Instrum. Methods Phys. Res. B **147**, 361 (1999).
[20] V. Borodin, K.-H. Heinig, and B. Schmidt, Nucl. Instrum. Methods Phys. Res. B **147**, 286 (1999).
[21] D. Williamson and S. Deb, J. Appl. Phys. **54**, 2588 (1983).
[22] N. Benczer-Koller, G. S. Collins, T. Kachnowski, and M. Pasternak, Phys. Rev. B **19**, 1369 (1979).
[23] G. Principi, A. Maddalena, A. Gupta, F. Geotti-Bianchini, S. Hreglich, and M. Verità, Nucl. Instrum. Methods Phys. Res. B **76**, 215 (1993).
[24] C. Hohenemser, Phys. Rev. **139**, A185 (1965).
[25] G. Koops, URL http://www.fys.kuleuven.ac.be/iks/nvsf/Files/thesis-gerhard.pdf (2001).
[26] S. Dickson and J. Mullen, Phys. Rev. B **58**, 5972 (1998).
[27] L. Nanver, G. Weyer, and B. Deutch, Phys. Status Solidi A **61**, K29 (1980).
[28] L. Nanver, G. Weyer, and B. I. Deutch, Z. Phys. B: Condens. Matter **47**, 103 (1982).
[29] K. Williams, C. Johnson, O. Nikolov, M. Thomas, J. Johnson, and J. Greengrass, J. Non-Cryst. Solids **242**, 183 (1998).
[30] K. Bourdelle, A. Johansen, and E. Johnson, Nucl. Instrum. Methods Phys. Res. B **118**, 478 (1996).
[31] T. Bachels, H. Güntherodt, and R. Schäfer, Phys. Rev. Lett. **85**, 1250 (2000).
[32] K. Unruh, T. Huber, and C. Huber, Phys. Rev. B **48**, 9021 (1993).
[33] F. Ercolessi, W. Andreoni, and E. Tosatti, Phys. Rev. Lett. **66**, 911 (1991).
[34] S. Lai, J. Guo, V. Petrova, G. Ramanath, and L. Allen, Phys. Rev. Lett. **77**, 99 (1996).
[35] H. Lamb, Proc. London Math. Soc. **13**, 187 (1882).
[36] A. Tamura and T. Ichinokawa, J. Phys. C **16**, 4779 (1983).